Acta Biomaterialia 8 (2012) 3349–3359

Contents lists available at SciVerse ScienceDirect

Acta Biomaterialia

journal homepage: www.elsevier.com/locate/actabiomat

Cohesive behavior of soft biological adhesives: Experiments and modeling

A. Khayer Dastjerdi [a], M. Pagano [a], M.T. Kaartinen [b,c], M.D. McKee [b,d], F. Barthelat [a,*]

[a] Department of Mechanical Engineering, McGill University, 817 Sherbrooke Street West, Montreal, Quebec, Canada H3A 2K6
[b] Faculty of Dentistry, McGill University, Montreal, Quebec, Canada
[c] Faculty of Medicine, Division of Experimental Medicine, McGill University, Montreal, Quebec, Canada
[d] Department of Anatomy and Cell Biology, McGill University, Montreal, Quebec, Canada

ARTICLE INFO

Article history:
Received 25 January 2012
Received in revised form 18 April 2012
Accepted 8 May 2012
Available online 12 May 2012

Keywords:
Soft biological adhesives
Fibrin
Fracture toughness
Cohesive law
Eight-chain model

ABSTRACT

Extracellular proteins play a key role in generating and maintaining cohesion and adhesion in biological tissues. These "natural glues" are involved in vital biological processes such as blood clotting, wound healing and maintaining the structural integrity of tissues. Macromolecular assemblies of proteins can be functionally stabilized in a variety of ways in situ that include ionic interactions as well as covalent crosslinking to form protein networks that can extend both within and between tissues. Within tissues, myriad cohesive forces are required to preserve tissue integrity and function, as are additional appropriate adhesive forces at interfaces both within and between tissues of differing composition. While the mechanics of some key structural adhesive proteins have been characterized in tensile experiments at both the macroscopic and single protein levels, the fracture toughness of thin proteinaceous interfaces has never been directly measured. Here, we describe a novel and simple approach to measure the cohesive behavior and toughness of thin layers of proteinaceous adhesives. The test is based on the standard double-cantilever beam test used for engineering adhesives, which was adapted to take into account the high compliance of the interface compared with the beams. This new "rigid double-cantilever beam" method enables stable crack propagation through an interfacial protein layer, and provides a direct way to measure its full traction–separation curve. The method does not require any assumption of the shape of the cohesive law, and the results provide abundant information contributing to understanding the structural, chemical and molecular mechanisms acting in biological adhesion. As an example, results are presented using this method for thin films of fibrin—a protein involved in blood clotting and used clinically as a tissue bio-adhesive after surgery—with the effects of calcium and crosslinking by Factor XIII being examined. Finally, a simple model is proposed, demonstrating how a bell-shaped cohesive law forms during the failure of the fibrin interface based on an eight-chain model whose structure degrades and changes configuration with stress.

1. Introduction

High-performance biological adhesives composed of proteins and/or polysaccharides are found in essentially all organisms [1]. These "bio-glues" vary extensively in structure and capabilities according to their function and performance requirements [2,3]. In general, bio-glues are deformable and can dissipate a significant amount of energy [4,5], and they can adhere to a variety of surfaces [1]. For instance, in humans, a fibrin network forms after bleeding following tissue trauma. Fibrin is a natural adhesive which can adhere to soft and hard tissues and withstand the stress imposed by pulsating blood pressure and ultimately stop bleeding [6]. Other examples include mussel, which can secret a high-performance proteinaceous adhesive (3,4-dihydroxyphenylalanine) to anchor themselves to rocks in order to resist the shear forces of tidal currents and waves [7]. Biological adhesives also ensure the intrinsic cohesion of key structural tissues such as bone, tooth enamel, dentin and cementum, and seashells. These tissues are composite materials consisting of both organic and inorganic phases, often with fibrillar elements such as collagen forming a scaffold within which mineral nano-crystallites are deposited, all of which are held together by specific non-collagenous proteins. For instance, in bone, the cohesion of collagen fibrils is ensured by bio-adhesive non-collagenous proteins [8]. Optimal deformability, strength and toughness of these bio-glues are therefore critical to the overall mechanical performance of mineralized tissues such as bone. While little is known about which protein molecules maintain the cohesion of bone, recent experiments have suggested that osteopontin may be such a key adhesive protein [9]. Transgenic mice lacking osteopontin have bones with a 30% decrease in fracture toughness independent of bone mineral density, a traditionally

* Corresponding author. Tel.: +1 514 398 6318; fax: +1 514 398 7365.
E-mail address: francois.barthelat@mcgill.ca (F. Barthelat).

1742-7061/$ - see front matter © 2012 Acta Materialia Inc. Published by Elsevier Ltd. All rights reserved.
http://dx.doi.org/10.1016/j.actbio.2012.05.005

used indicator of bone fragility [10]. As another example where extracellular bio-adhesives appear to be particularly important, the organic constituents of seashell nacre serve as a nanometers-thick mortar maintaining the integrity of microscopic mineral tablets. This organic phase, despite comprising less than 5% of the nacre volume, is critical to shell toughness [5]. In particular, the soft interface enables micro-motion (sliding) of mineral tablets on one another when under external stress, generating large deformation, energy dissipation and toughness [11]. Single-molecule force spectroscopy using atomic force microscopy (AFM) has revealed how sacrificial bonds and hidden lengths within adhesive biological molecules in bone or nacre can generate toughness at the nanoscale [4,12]. Transmission electron microscopy observations have also confirmed that the organic phase of nacre can dissipate a substantial amount of energy through protein unfolding [13]. The deformation and stretching of certain proteins found in bio-glues are reversible, because of unfolding and refolding of coiled sections of the protein chains. This process dissipates energy and provides self-healing capabilities across interfaces [13]. There is now a large body of work involving "pulling" experiments on single proteins using AFM. While these experiments are highly useful in revealing fundamental molecular mechanisms underlying adhesion, the combination of substrates that can be used is limited by the type of chemistry available to functionalize the AFM tip. In addition, how these single protein mechanisms translate into fracture toughness of the adhesive interface as a whole is not clear, because macroscale toughness is also a function of the molecular density of the network, its three-dimensional structure and subunit conformation, as well as the chemical affinity for the apposing substrates. Few experimental techniques have been developed for testing the interfacial fracture toughness of adhesive interfaces. These include the blister test [14], the indentation test [15] and the double cantilever beam test (DCB) [16]. These tests were originally developed for strong industrial adhesives and cannot be directly used for measuring the toughness of biological interfaces because of the weak nature of biological adhesives. For instance, Sierra et al. [14] used the blister test for measuring the interfacial toughness of fibrin sealant by assuming a linear elastic behavior for fibrin, which is not truly realistic. In addition, these techniques only measure a single value for toughness and do not provide details about failure parameters such as extensibility or maximum traction. Another approach consists of combining the DCB test with imaging techniques to determine the cohesive behavior of strong industrial adhesives [17]. The present work proposes a new experimental approach to measure the cohesive behavior of proteinaceous interfaces as well as their toughness from a fracture mechanics perspective, where the energy required to propagate an existing crack is measured. The technique is easy to implement, and measures the extensibility, strength and stiffness of the interface. This type of information is useful for understanding the origin of, and possibly optimizing, the toughness of biological adhesives (including high extensibility, high strength or a combination of both). To illustrate this method, fibrin was chosen because it is used extensively in surgical procedures [18,19] and in tissue engineering [20]. This new method could contribute towards optimizing the chemical preparation and structure of this protein in order to achieve maximum toughness.

2. Fracture toughness and the rigid double-cantilever beam method

Fracture toughness is a material property which characterizes how well a material can resist crack propagation. Virtually all materials (and interfaces) contain microscopic defects and flaws which may propagate into long cracks and eventually lead to complete, catastrophic fracture of a material. How well a material can resist cracking and tolerate the presence of cracks directly affects strength, reliability and energy absorption, which are all critical properties for a structural material such as bone. The fracture toughness of engineered materials is routinely measured using well-established, standardized tests [21]. In these tests, typically, a sample of well-defined geometry containing a pre-crack is mechanically loaded such that the crack propagates and fractures the sample. In the context of linear elastic fracture mechanics, the fracture toughness is computed from the load which triggers crack propagation and from the geometry of the specimen (ASTM E399). Similarly, the fracture toughness of engineering adhesives can also be measured, typically using the double-cantilever beam (DCB) test configuration—a useful, widely used approach for obtaining interfacial fracture toughness measurements in the "opening" fracture mode (mode I) [16,22]. A DCB specimen consists of two flat beams bonded by a thin layer of adhesive in such a way that a section of each beam remains free of adhesive to generate a pre-crack (Fig. 1a). The system is then loaded by pulling the free ends of the two beams in a direction normal to the fracture surface in order to extend the pre-crack along the interface of the two beams. The elastic energy stored in the beams is released upon crack extension and can be calculated in order to measure the toughness (energy required to extend a crack) of the adhesive [16,21]. This method is adequate for engineered adhesives such as epoxies and polyuria, which are relatively stiff and strong compared with the flexible beams. In contrast, the method is much less reliable for soft glues, such as proposed for proteins sandwiched between much stiffer substrates (Fig. 1b). The assumption that the beams are flexible is inappropriate in the case of highly deformable adhesives, since the adhesives themselves are much more compliant than the beams. In this case, the elastic energy is stored in the adhesive itself instead of in the beams.

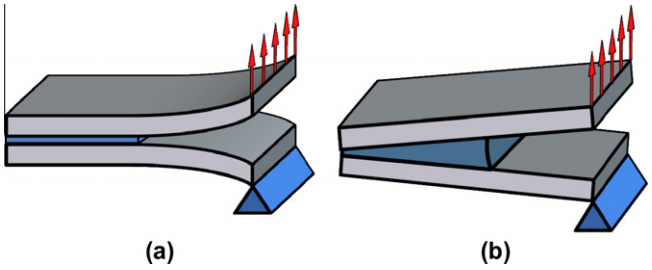

Fig. 1. (a) Traditional DCB test, in which the mechanical energy is stored predominantly in the beams; (b) RDCB, in which the mechanical energy is stored predominantly in the adhesive itself.

Therefore, a "rigid double-cantilever beam" method (RDCB) is introduced to measure properly the toughness of soft bio-adhesives (Fig. 1b). This configuration enables direct control over crack opening, and promotes stable crack propagation at the interface. Moreover, it provides a direct way to measure accurately the cohesive behavior (traction–separation function, or cohesive law) of the soft adhesive.

2.1. Sample preparation and RDCB testing

In the following sections, the RDCB method is presented and validated using commercial, office double-sided tape (3M Scotch tape) on glass. The double-sided tape is composed of a cellulose acetate film coated on both sides with acrylic glue, forming a 100-μm-thick sandwich structure. Small RDCB samples were made of two $22 \times 3 \times 5$ mm rectangular glass beams, cut from microscope slides using a precision diamond saw. A rectangular patch

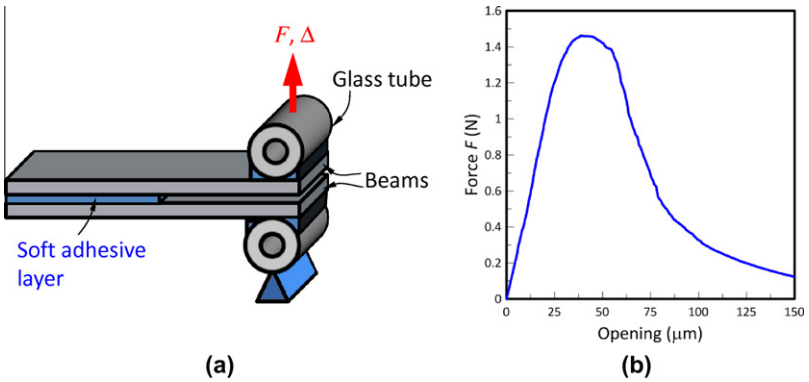

Fig. 2. (a) Schematic illustration of a RDCB specimen. An opening displacement Δ is imposed, while the opening force F is recorded; (b) a typical F–Δ curve obtained from tape-on-glass specimen.

of tape was placed between the two glass beams, and the assembly was completed by gluing a short glass tube at the ends of the two beams to facilitate beam separation (Fig. 2a). The RDCB sample was then placed in a miniature loading stage (Ernest F. Fullam, Latham, NY) operated horizontally. Two steel pins mounted on each of the moving crossheads were used to apply a tensile force on the specimen through the glass tubes. The opening displacement Δ was increased at a fixed rate of 3 μm s^{-1}, while the force F was recorded with a load cell. A typical load–opening curve for the tape-on-glass system is shown in Fig. 2b. The curve initially showed a linear trend and softening at the point where the crack started to propagate. Softening continued until the maximum force was reached, which was followed by a gradual decrease of the force until complete failure of the interface. This bell-shaped curve indicates that the crack propagated in a stable fashion, implying that powerful toughening mechanisms are at work in this particular adhesive, possibly through the formation of ligaments spanning the crack faces. Post-test examination revealed that the crack propagated along one of the interfaces between the tape and the glass substrate (interfacial fracture).

2.2. Analysis of RDCB test results

The RDCB analysis relies on the rigidity of the substrates: the crack faces remain straight and the crack opening displacement δ can be directly related to the crack mouth displacement Δ (Fig. 3). The assumption of rigid beams can be verified by writing the stiffness of a cantilever beam in bending:

$$S = \frac{3EI}{a_0^3} \tag{1}$$

where E is the modulus of the beam (for glass E = 72 GPa, and for polycarbonate E = 2.5 GPa), I is the area moment of inertia, and a_0 is the initial crack length. Since there are two beams, the stiffnesses of the RDCB beams used in this work are $S/2$ = 1200 N mm^{-1} for tape-on-glass case, $S/2$ = 150 N mm^{-1} for fibrin-on-HAP and $S/2$ = 90 N mm^{-1} for fibrin-on-collagen. The typical initial stiffness from the experiments on tape-on-glass, fibrin-on-HAP and fibrin-on-collagen cases is ~55, 5 and 8 N mm^{-1}, respectively, which is much softer than the beams. If the adhesive is soft enough, the deflection of the beams can therefore be neglected over the deflection of the adhesive itself. Similarly, the energy stored in the beams is negligible compared with the energy stored in the adhesive itself. This can be verified by writing the elastic energy stored in a cantilever beams of the RDCB specimen [23]:

$$U = \frac{1}{2}\frac{P^2}{S} = \frac{1}{2}\frac{P^2 a_0^3}{3EI} \tag{2}$$

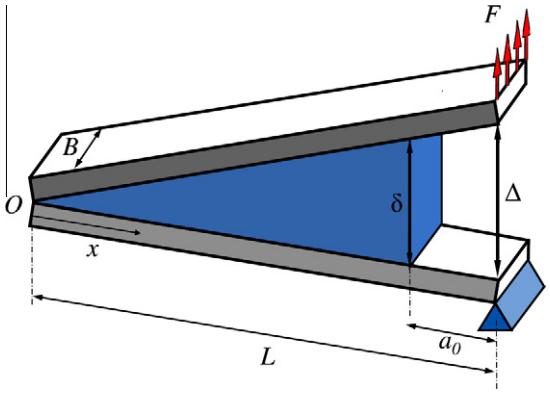

Fig. 3. Schematic illustration of RDCB specimen with relevant dimensions.

Using the parameters above, the elastic energy stored in the two beams ($2U$) can be estimated at the typical maximum load measured for each case: $2U = 5.9 \times 10^{-7}$ J for tape-on-glass, $2U = 2.5 \times 10^{-8}$ J for fibrin-on-HAP, and $2U = 1.0 \times 10^{-6}$ J for fibrin-on-collagen. These energies represent at most 0.5% of the total energy dissipated in the typical experiments presented here. The energy stored in the beam is therefore negligible compared with the amount of energy involved in fracturing the adhesive.

With the assumption of rigid beams, the analysis of the RDCB starts by balancing the moment exerted by the closure force exerted by the adhesive with the moment generated by the applied force F (about point O), giving

$$B\int_0^{L-a_0} xt(x)dx = LF \tag{3}$$

where F is the applied force, L and B are the length and width of the beams, x is the distance from point O and a_0 is the initial crack length. Since the beams are considered rigid, the opening u at any point at distance x from point O is given by:

$$u = \frac{x}{L}\Delta \tag{4}$$

where Δ is the crack mouth displacement (separation at the ends of the beams). Eq. (4) is used for a change of variables on the integral in Eq. (3) to yield:

$$\left(\frac{L}{\Delta}\right)^2 \int_0^{\delta} ut(u)du = \frac{L}{B}F \tag{5}$$

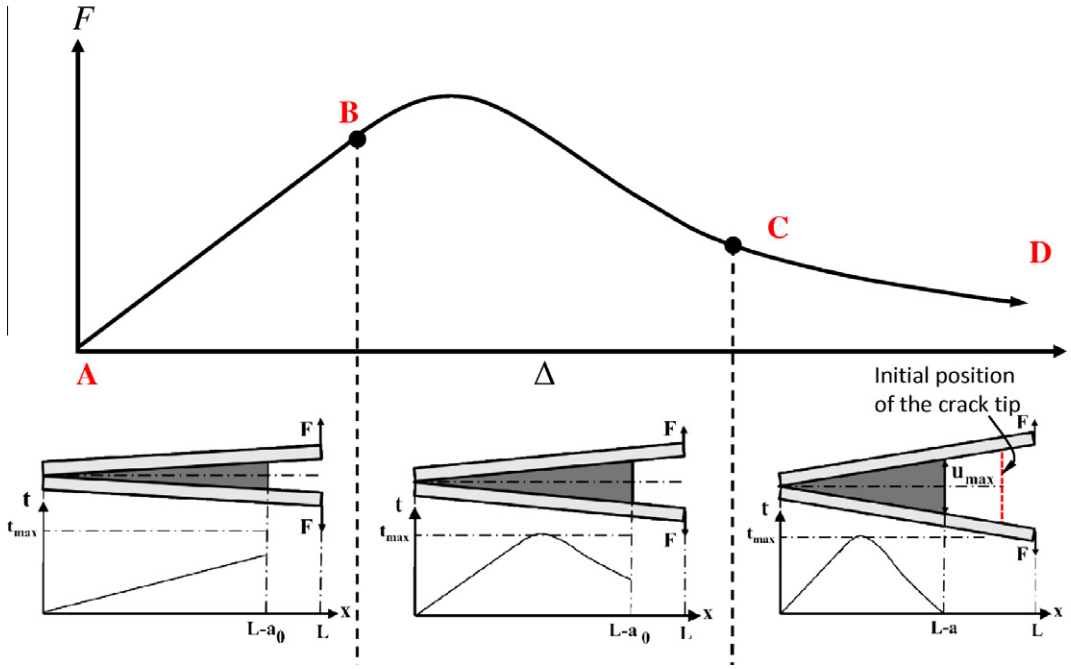

Fig. 4. Graphical depiction of how Eq. (7) is applied to compute the cohesive law as function of the F–Δ curve.

The objective is to determine the traction function $t(u)$ without any assumption about the shape of cohesive law. To this end, Eq. (5) is derived with respect to Δ, giving after rearranging

$$t(\delta) = \frac{1}{\Delta}\frac{L}{B(L-a_0)^2}\frac{d}{d\Delta}(\Delta^2 F) \tag{6}$$

Or, in a more convenient form

$$t(\delta) = \frac{L}{B(L-a_0)^2}\left(2F + \Delta\frac{dF}{d\Delta}\right) \tag{7}$$

Eq. (7) therefore provides a simple approach to the direct determination of the traction generated by the glue onto the substrate as function of separation, which constitutes the cohesive law of the interface. Cohesive zone modeling is a powerful technique for simulating crack initiation and growth and is often used to model fracture and fragmentation processes in metallic, polymeric and ceramic materials and their composites [24]. The full cohesive law provides more information than a simple measurement of toughness, while the toughness of the interface G_c is simply given by the area under the cohesive law.

The application of the equation is depicted graphically in Fig. 4. For a given F and Δ, δ is computed by applying Eq. (4) at the crack tip ($x = L - a_0$):

$$\delta = \frac{L-a_0}{L}\Delta \tag{8}$$

The traction at the tip can then be computed using Eq. (7). By repeating the process over the entire experimental F–Δ curve, the complete cohesive law can be obtained.

Fig. 5 shows the experimental F–Δ curves for tape-on-glass and the corresponding cohesive laws computed with Eq. (7). The initial region of the cohesive law is linear, corresponding to the elastic deformation of the interface. At a separation of ~10 μm the interface softens, as damage accumulates in the adhesive. Damage accumulation continues until the cohesive law reaches a maximum (the cohesive strength, in this case t_{max} = 90–100 kPa) after which the interface continues to soften as damage increases. The cohesive traction vanishes when the opening reaches the maximum separation distance u_{max} = 30–55 μmin this case). Once the cohesive law is computed, the toughness of the interface is then simply given by the area under the cohesive law:

$$J_{IC} = \int_0^\infty t(u)du \tag{9}$$

The toughness given by Eq. (9) is equal to the work-of-fracture, defined as the area under the (F–Δ) divided by the initial surface area of the adhesive (i.e., work-of-fracture measures the energy required to separate a unit surface of adhesive). In the case of tape-on-glass, a toughness of $J_{IC} = 2.4 \pm 0.4$ J m^{-2} was measured. For validation of this result, the toughness of tape-on-glass was also measured, using a standard peel test (ASTM D6862-04), which gave a reference toughness of 2.5 ± 0.3 J m^{-2} for the interface. The values given by the RDCB and peel tests are comparable within experimental errors.

Natural protein adhesives such as fibrin consist of protein networks saturated with water. In order to assess the contribution of water to the adhesion of the interface, a control experiment was performed on distilled water only, sandwiched between two glass beams forming a RDCB configuration. The typical cohesive law of water-on-glass is presented in Fig. 6, corresponding to a cohesive work of 0.18 ± 0.03 J m^{-2}. This corresponds to only 4% of the typical fracture toughness of fibrin network (presented below), and demonstrates that cohesive effects associated with surface tension of the water has only a negligible effect on the adhesion of hydrated fibrin networks.

3. Adhesion of fibrin

The RDCB method as developed for this work was designed to measure the toughness of soft biological adhesives. This work investigated fibrin, a key protein in the physiological formation of blood clots and in the induction of wound healing processes. Fibrin is widely used as a surgical adhesive and clinical bonding agent [18,19]. Fibrinogen, the precursor of fibrin, is a circulating glycoprotein synthesized in the liver [25]. Fibrinogen, when

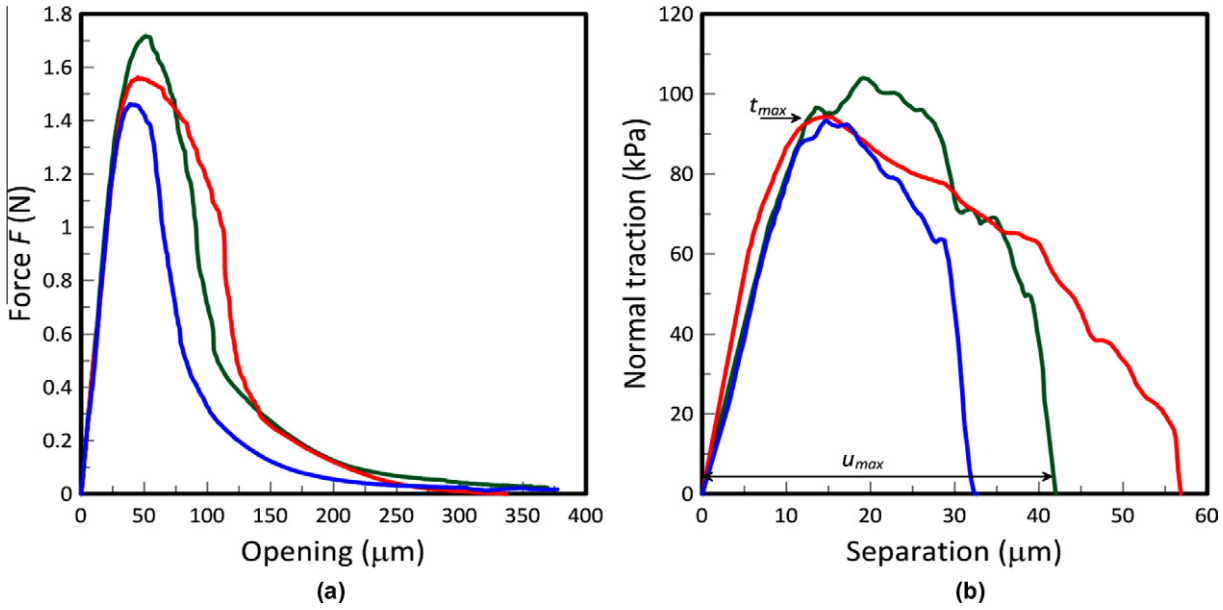

Fig. 5. (a) Typical F–Δ curves from the tape-on-glass experiment; (b) corresponding cohesive laws determined from the RDCB model.

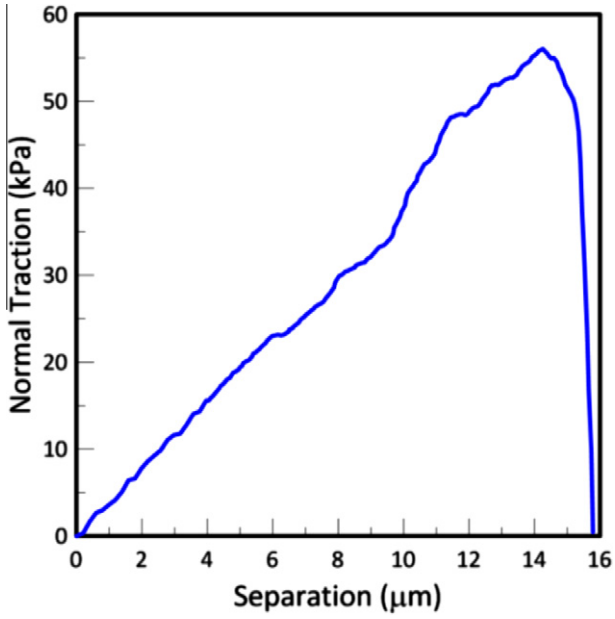

Fig. 6. Cohesive law of water-on-glass test obtained using RDCB technique.

cleaved by thrombin, undergoes a self-assembly process to form a fibrin network. Thrombin is an enzyme that proteolytically activates a number of coagulation cascade factors [26,27], and it cleaves two peptide regions within fibrinogen, which allows spontaneous intermolecular fibrinogen interactions to occur. The highly adhesive fibrin network formed in this way acts as a tissue adhesive, as well as capturing and activating platelets to form a blood clot that stops bleeding [28,29]. Factor XIII is a member of the transglutaminase family of enzymes, which catalyze calcium-dependent formation of covalent crosslinks between glutamine and lysine residues of substrate proteins [30,31]. Factor XIII's cross-linking function is activated by thrombin, and covalent crosslinking of the fibrin network greatly increases the strength, stability and overall mechanical properties of the fibrin network [32,33].

In the present work, the adhesion of fibrin onto a layer of hydroxyapatite (HAP, the mineral phase of bone) and onto sheets of type I collagen (the major extracellular matrix protein fibril found in most human tissues) was measured using the new RDCB approach. HAP substrates were obtained from 1-mm-thick Osteologic™ coverslips made of transparent quartz glass coated with a 600-nm-film of HAP, as supplied by the manufacturer (BD Bioscience, Mississauga, ON, Canada). The 1-mm-thick coverslips were first cut into 12×2 mm rectangular strips using a high-precision diamond saw (Struers, Mississauga, ON, Canada). Cutting was performed under dry conditions to ensure that the HAP coating was not exposed to aqueous conditions. The morphology of the coated surface was characterized by AFM (Veeco Dimension V, Santa Barbara, CA) (Fig. 7a). AFM scans of different locations on the coverslips revealed that the surface was uniformly coated, displaying a smooth surface (surface roughness 50 ± 6 nm, measured from AFM data). Type I collagen substrates were prepared from individual fish scales from a fresh striped bass (*Morone saxatilis*), acquired from a fish supplier (Nature's Catch, Clarksdale, MS, USA). The fish scale was gently dissected with a fresh razor blade from the underside to yield ~100-μm-thick sheets of type I collagen with a crossply structure (Fig. 7b) [34]. This preparation method produced flat layers of dense type I collagen, which were then glued onto 20×3 mm polycarbonate beams using cyanoacrylate glue. Since the binding between cyanoacrylate glue and glass was not strong enough, 3-mm-thick polycarbonate beams were used to ensure that the collagen layer did not de-bond from the substrate during the course of fracture test. Fig. 7b shows a scanning electron micrography (SEM) image of the collagen layer revealing the crossply arrangement of type I collagen fibrils characteristic of the structure of fish scales [35]. The collagen prepared in this fashion therefore presented relatively smooth surfaces consisting of exposed surfaces of fibrils. The preparation of the beams was completed by gluing a short section of a hollow glass tube at the end of the beam (Fig. 2a). Fibrin was prepared from bovine fibrinogen (F8630) with thrombin (T4648) incubation (proteins purchased from Sigma–Aldrich, St-Louis, MO, USA). The thrombin was dissolved in distilled and deionized (Milli-Q, Millipore, Billerica, MA, USA) water or calcium chloride solution to a concentration of 10.7 U ml^{-1}. Fibrinogen was then dissolved in 0.9% NaCl saline to a 50 mg ml^{-1} concentration. The fibrinogen and thrombin

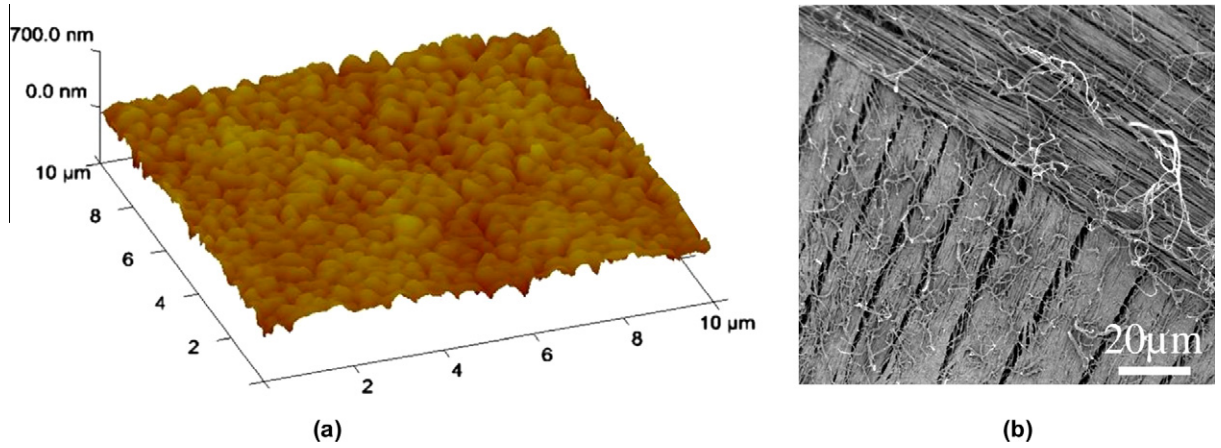

Fig. 7. (a) Three-dimensional (3D) AFM image of the HAP coating of the Osteologic™ coverslips; (b) SEM image of a peeled collagen layer showing the crossply structure of collagen fibril arrangement.

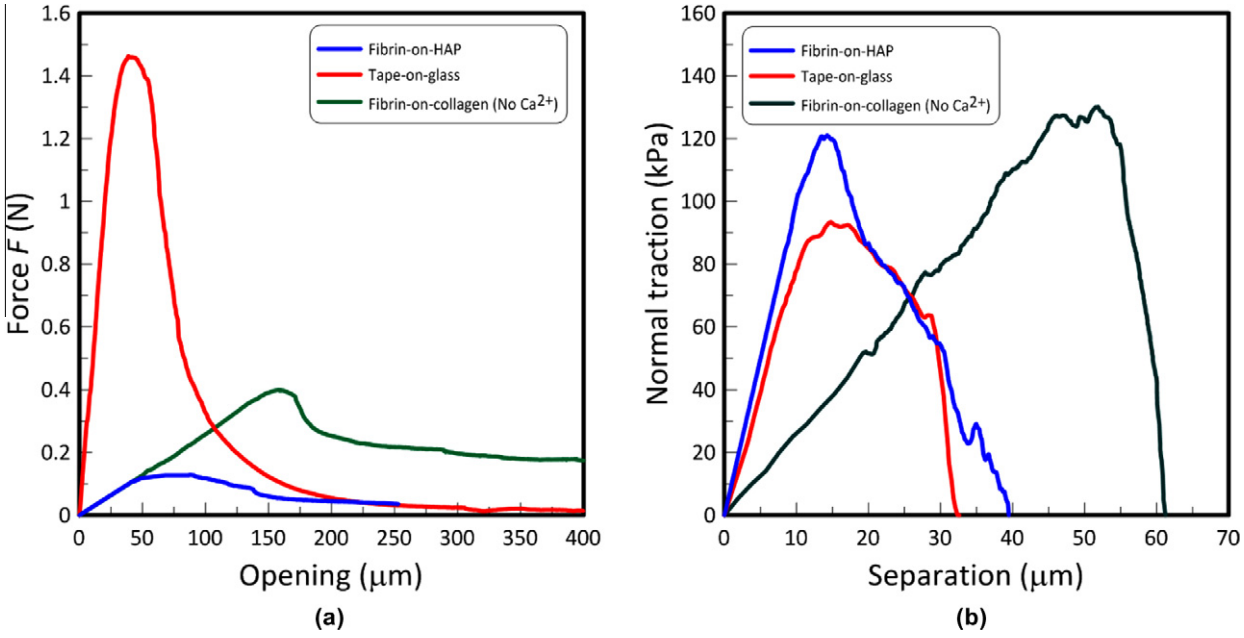

Fig. 8. (a) Typical F–Δ curves from different adhesive–substrate combinations, and (b) corresponding cohesive laws determined from the RDCB model.

solutions were then combined and mixed in a vortex apparatus (for ~1 s) with an equal volumetric ratio, in order to form a viscous fibrin solution. A small volume (5 μl) of this solution was then immediately applied to approximately half the length of the beam-mounted substrates. Another beam was then placed on top of the first one, completing the RDCB sample assembly. The specimens were then placed in a custom-made humid chamber and incubated for 30 min at 37 °C. Throughout the incubation process, a 60 g weight was applied to generate pressure on the interface. The samples were then immediately tested following the procedure described above. For each fibrin group, 10 samples were tested.

To investigate the deflection and energy stored in the cyanoacrylate and collagen layer, a control experiment was conducted on a layer of collagen glued between two polycarbonate beams with cyanoacrylate glue. Because of the high toughness of collagen, the crack propagated between the cyanoacrylate and the polycarbonate substrate at a force of 2 N. Nevertheless, the result up to failure could be used to estimate the stiffness of the beams, collagen and cyanoacrylate layers (85 N mm^{-1}), which is more than 10 times stiffer than a fibrin layer. In addition, the control experiment can be used to estimate the energy stored in the cyanoacrylate and collagen layers at an opening force of 0.4 N, which is the force required to fracture fibrin (Fig. 7a). Assuming that the energy stored in the polycarbonate beams is negligible, the energy stored in the collagen and cyanoacrylate layers is 2×10^{-6} J. In the fibrin-on-collagen experiment, two layers of collagens were used, and a conservative estimate of the energy stored in the cyanoacrylate and collagen is therefore 4×10^{-6} J, which represents only 2.4% of total energy dissipated during the course of crack propagation in fibrin-on-collagen tests. This configuration therefore ensures that more than 97% of the energy injected in the RDCB specimen is dissipated towards propagating the crack in the fibrin interface. Fig. 8a displays representative F–Δ curves for fibrin-on-HAP, fibrin-on-collagen and tape-on-glass (for comparison). All curves display a bell shape characteristic of stable crack propagation, and Fig. 8b shows the corresponding cohesive laws. Fibrin-on-HAP displays a toughness on average twice as high as that of tape-on-glass, and

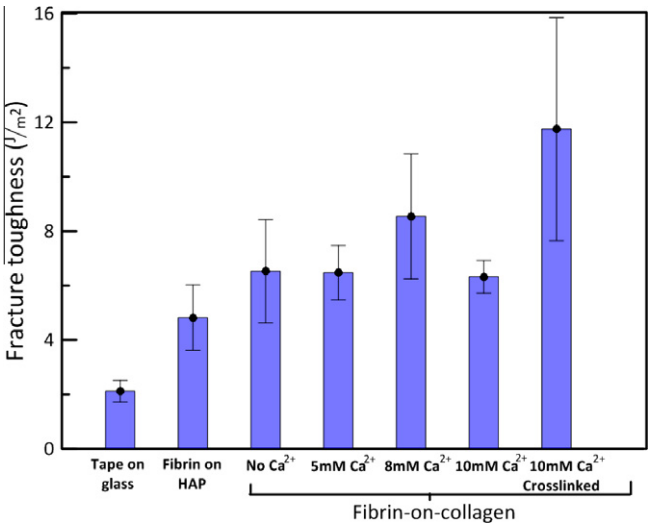

Fig. 9. Summary of toughness for the interfaces tested in this work.

fibrin-on-collagen toughness is even greater—~30% tougher than fibrin-on-HAP (the results for toughness are summarized in Fig. 9). This difference can be explained by examining the cohesive laws: fibrin-on-HAP and tape-on-glass have about the same bell-shaped curves and the same average maximum separation (25 μm), but fibrin-on-HAP is slightly stronger (Fig. 8), thereby leading to greater toughness. The surface separations in these tests are in the order of micrometers, while reported values for single fibrin fiber pull-out distance is in the order of nanometers. This is to be expected, since the adhesive consists of a network formed of a large number of individual fibers. Post-test exploration of the fracture surface of the fibrin-on-HAP specimens using optical microscopy showed a mixed-mode failure (cohesive and adhesive), with the latter being dominant (Fig. 10). In cohesive failure, cracks propagate within the adhesive (here fibrin), while in the other case, cracks extend to the adhesive/substrate interface. Referring to these images, it can be inferred that the binding between the adhesive and substrate is weaker than the internal binding of the adhesive itself. Fibrin-on-collagen showed, on average, a strength similar to that of fibrin-on-HAP, but with larger separations

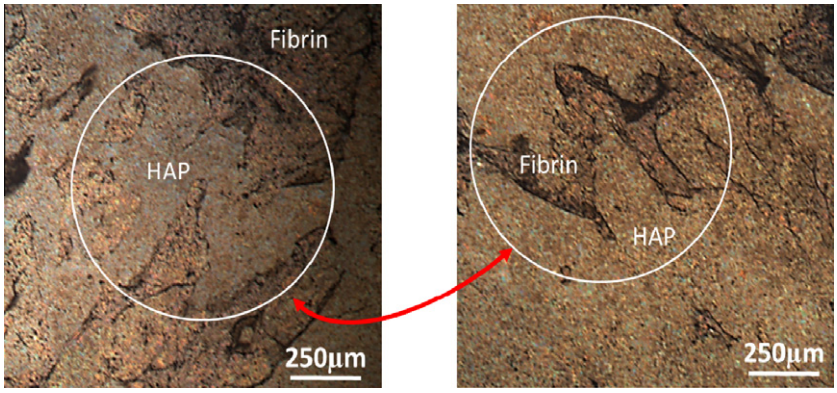

Fig. 10. Optical images of a fibrin-on-HAP specimen showing the two fracture surfaces after testing. The white circle highlights a region where an "island" of fibrin was detached from one surface (left panel), and the corresponding region was located on the other surface (right panel). The overall failure mode is cohesive (i.e., the crack propagates at the interfaces between the adhesive and the substrates).

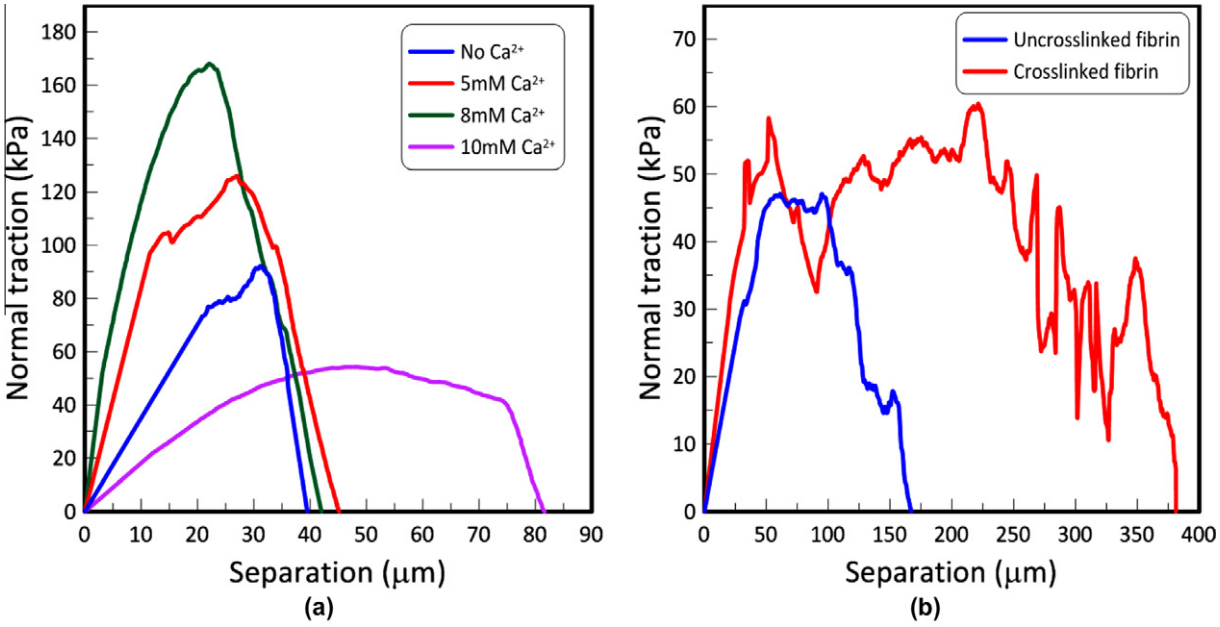

Fig. 11. Effects of (a) calcium concentration and (b) crosslinking on the cohesive behavior of fibrin on collagen.

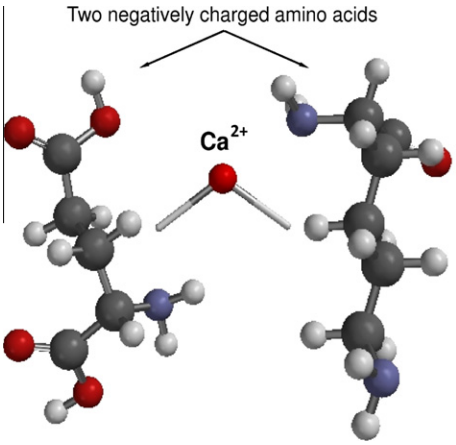

Fig. 12. A schematic of the bridging of two negatively charged amino acids by Ca cation forming a salt bridge.

(60 μm), which explains the greater toughness of fibrin-on-collagen.

The relatively poor adhesion of fibrin-on-HAP can be explained by the weak nature of the electrostatic interactions between calcium- or phosphate-rich crystal faces of HAP and electrically charged residues of the fibrin network [36,37]. In the case of fibrin-on-collagen, interaction of the electrically charged and/or polar amino acids of these two proteins could lead to a greater affinity and stronger bond. The collagen substrate may also provide additional deformation and energy dissipation compared with the stiff HAP substrate, thereby leading to lower stiffness of the cohesive law in its linear part (Fig. 8b).

The effect of calcium concentration, which is known to have demonstrable effects on the structure and strength of fibrin [33], was also investigated. Calcium chloride was introduced into the thrombin solution before mixing at concentrations of 5, 8 and 10 mM, while the rest of the sample preparation followed the same protocol as described above (for these experiments, only the collagen substrate was used). Typical cohesive laws are shown in Fig. 11a, and these show that an increase in calcium concentration (up to ~8 mM) enhances the average stiffness and strength of the fibrin/collagen interface, while only slightly affecting the maximum separation distances (Fig. 11). As a result, the toughness increases, as shown in Fig. 9. This trend is consistent with previous observations on calcium ions increasing the diameter and length of the fibrin fibrils [33], which was shown to translate into greater overall strength for the network [6]. In addition, calcium ions probably enhance the adhesion between the electrically charged amino acids of the fibrin and collagen. The binding of Ca^{2+} to the negatively charged sites of these two proteins can reverse their charges, making them potential sites for binding to other acidic residues of the proteins (salt bridge formation) (Fig. 12) [38–40]. The present results showed a decrease in strength beyond addition of 8 mM Ca^{2+}, which is also consistent with previous studies [41,42]. This decrease in strength performance could be explained by the formation of defects attributable to the increase in $CaCl_2$ concentration, which could loosen the fibrin network, making it weaker but more extensible [41,42]. Interestingly, the cohesive law corresponding to fibrin with no added calcium ions and with 5 and 8 mM calcium content all failed in the same way, with an ultimate separation of ~40 μm. This observation supports a scenario where calcium ions form salt bridges with the fibrin network, stiffening and strengthening the adhesive. Upon failure, the chains remain intact, but the salt bridges break, so that a fibrin adhesive with 8 mM calcium chloride results in the same conformation as fibrin without addition of calcium. The area between these cohesive curves and the cohesive law of fibrin without added calcium yields the energy dissipated through salt bridge rupture which finally leads to an increase in the fracture toughness of the interface. Formation and rupture of calcium-ion-mediated bonds and repeated energy dissipation through this process have been observed at the nano-scale using AFM [38].

Finally, the effect of covalent crosslinking on the fracture behavior of the fibrin network was examined. Fibrin was prepared as described above, and crosslinking of fibrin was induced by adding human Factor XIII (Innovative Research, Novi, MI, USA) to the fibrinogen solution and then combining and mixing it with the thrombin solution. In addition to inducing fibrin formation from

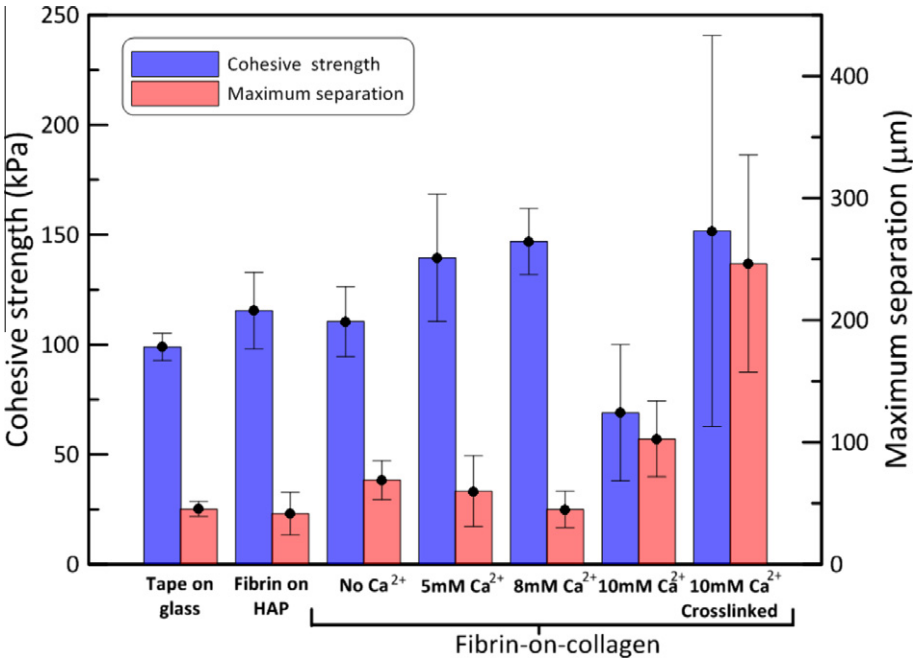

Fig. 13. Summary of cohesive strengths and maximum separations for the interfaces tested.

fibrinogen, thrombin also activates Factor XIII, where 10 mM $CaCl_2$ and a longer incubation time (2 h) are required for crosslinking; the final concentration of Factor XIII used was 20 μg ml^{-1}. In terms of toughness, crosslinked fibrin produced a jagged F–Δ curve, with indications of multiple crack arrests and additional toughening mechanisms resisting crack propagation.

The observed maximum opening displacement was substantially greater for crosslinked fibrin, which resulted in a doubling of the overall toughness (Fig. 9). High work-of-fracture could originate from two sources: (i) an increase in the strength [43] and extensibility [32] of the fibrin because of the crosslinking, and (ii) strong covalent binding at the collagen/fibrin interface. The crosslinking increases the strength of single fibrils, which is then translated into greater strength for the fibrin network [6]. However, covalent bonds that form between glutamine and lysine residues of collagen and fibrin (in the presence of calcium cations and Factor XIII) could transfer much external loading to the interface, thereby leading to greater extensibility of the interface [31].

The parameters of the cohesive law for different interfaces are summarized in Fig. 13. These results provide useful insight into the mechanics of adhesion. For example, despite the fact that both tape/glass and fibrin (5 mM $CaCl_2$)/collagen interfaces show approximately the same strength, the greater extensibility of the fibrin/collagen interface gives rise to a two- to threefold increase in the fracture toughness compared with that of the tape/glass interface. Also, two interfaces with the same toughness may follow a different cohesive law (i.e., different t_{max} and u_{max}). For example, fibrin (5 mM $CaCl_2$)/collagen and fibrin (10 mM $CaCl_2$)/collagen have about the same toughness, but fibrin (5 mM $CaCl_2$)/collagen achieves toughness with high cohesive strength, while fibrin (10 mM $CaCl_2$)/collagen achieves toughness with high extensibility. In such a case, the function of the adhesive determines which one is the most desirable. For example, high adhesive strength and stiffness are probably more beneficial to a blood clot which must not deform to obstruct blood flow. The RDCB technique, when combined with the cohesive zone model presented here, can therefore be used as an experimental bridge between molecular mechanics and fracture toughness. This technique can also be used to screen and customize bio-adhesives for actual applications in surgery, tissue reconstruction and tissue engineering.

4. Modeling fibrin network failure

Some of the experimental observations reported in the present study motivated the present authors to develop a simple model to capture the progressive failure of a fibrin network. While there is a

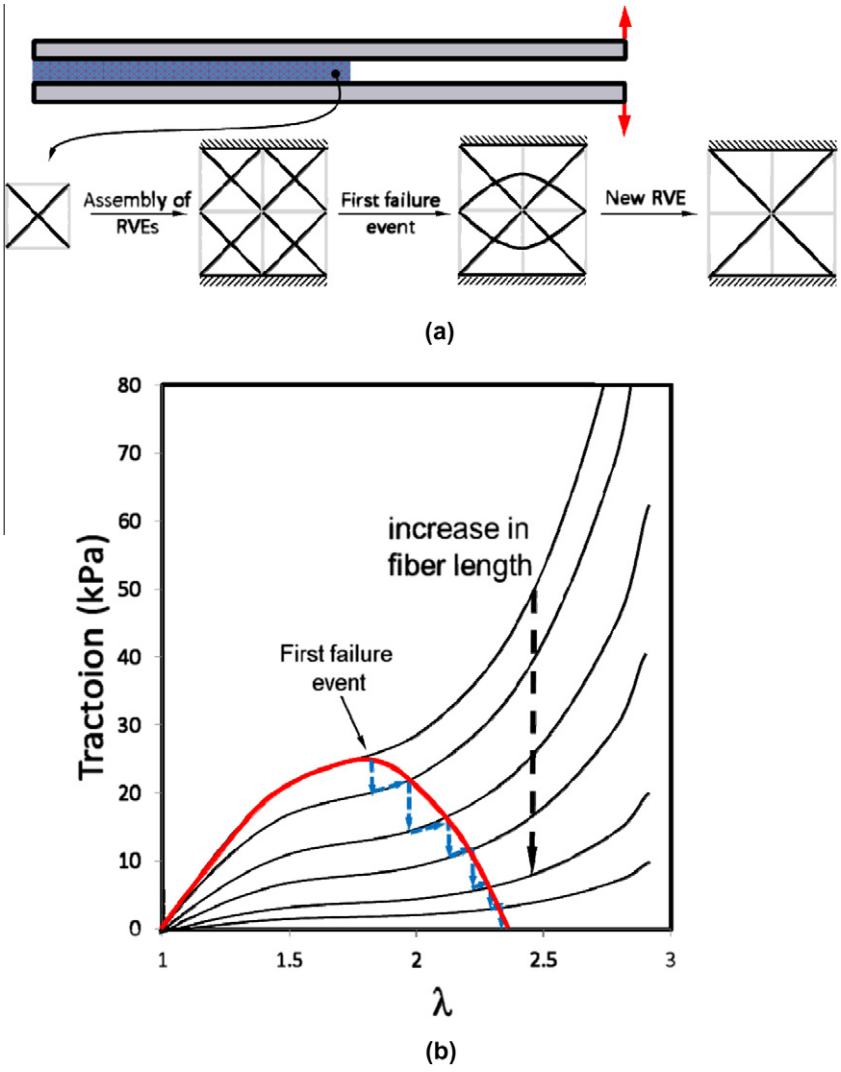

Fig. 14. (a) A two-dimensional (2D) schematic of RDCB specimen in which fibrin network is modeled with a 2D four-chain model. The 2D model simply shows how an RVE changes to another RVE with larger side length following the failure at the top and bottom middle pins; (b) traction–stretch curve of fibrin network with various fibril lengths. Successive failure events attributable to rupture in bonds results in a bell-shaped cohesive model.

substantial body of work on modeling the constitutive behavior of polymer networks (three-chain [44], eight-chain [45] and isotropic network models [46]), most of these models focus on elasticity. Such a model was recently modified to simulate the elastic behavior of fibrin [6]. In this model, the extension of an individual fibrin fibril at low stretch (before unfolding) is modeled by a simple linear spring. A worm-like-chain model is used to describe the unfolding state of the fibrin fibril deformation at high stretch. The energy stored in eight deformed fibrils was then related to the strain energy density of the macroscopic representative volume element (RVE). According to this model, the first Piola–Kirchhoff stress (defined as traction force per unit area of the undeformed body) in a uniaxial tension state is given by [6]

$$\sigma_{11}^{P} = \frac{vLF(\lambda_c)}{6\lambda_c}\left(1 - \frac{\lambda_*^2}{\lambda_1^2}\right) \tag{10}$$

where v, L and $F(\lambda_c)$ are the fibril density, the undeformed length of the fibrin fibril in the RVE, and the force–extension relation of the fibril, respectively. Fibril density is defined as the number of fibrils per unit reference volume. λ_c, λ_1, λ_* and λ_* denote the stretch of each fibril, of the RVE in loading direction, and of the RVE in transverse directions, respectively [6]. This model captures the stiffening of the fibrin network at large strains from structural parameters obtained from independent image analysis (other models which also capture stiffening in fibrin could have been used [46]). The cohesive laws measured on fibrin do not exhibit any stiffening, which was attributed to progressive de-cohesion from the substrate. A simple model is presented, which can qualitatively explain the softening of the fibrin network sandwiched between two substrates adhesive by progressive breakage of the salt bridges and network reconfiguration. For the sake of simplicity, a two-dimensional four-chain model representing the fibrin network is presented in Fig. 14a. The fibrin fibrils can branch, and are also "crosslinked" by salt bridges, which represent weak bonds for the network. Fig. 14a shows how the rupture of these pinning points (branching points or salt bridges) generates dangling sections of chains no longer carrying any external load. Hence, after the first failure event, the RVE of the structure changes conformation, so that a new RVE two times larger than the original RVE is needed to model the network. The same failure scenario progressively occurs at greater external loads and gives rise to a structure with larger fibrils and much lower effective fibril density (which is much weaker than the original structure). Although the fibril density is constant throughout the whole structure failure, the density of those fibrils resisting external loading (here called as effective fibril density v_e) reduces at an increasing rate during the failure. For a 3D network, v_e can easily be determined from the fibril length using

$$v_e = \frac{3\sqrt{3}}{L^3} \tag{11}$$

where L is the free length of the fibril between two crosslinks. Substituting Eq. (11) in Eq. (10), the first Piola–Kirchhoff stress becomes proportionally related to the inverse of L^2. Therefore, upon each failure event, the stress–stretch curve of the network shifts to a new path with lower stress level. Fig. 14b shows the stress–stretch curve of network structures with increasing fibril length, with all parameters of the model (except fibril density) taken from Ref.[6]. The red line in this figure indicates the path that the network follows, i.e., before failure it follows a stress–stretch curve which belongs to an intact network, then at the first failure point, the stress shifts to another curve which belongs to a network with greater fibril length, yet with much lower effective fibril density. This process continuously takes place up to the final failure, which is concurrent with the complete decohesion at the interface. In addition, in Fig. 14b traction vs stress is plotted in a manner in which the stretch can easily be converted to separation, provided that the thickness of the interface is known. This simple model could therefore explain the shape of the experimental cohesive law, and how the failure of the fibrin network (mainly de-cohesion from substrate) is associated with progressive breakage of salt bridges within the network.

5. Conclusion

The novel RDCB method presented here can be used to measure the adhesion of soft adhesives on a variety of substrates, and it is particularly well suited to the analysis of biological adhesives. Moreover, the RDCB yields the full cohesive law for the glued interface, without any initial assumption about the shape of that cohesive law. Compared with a single value for toughness, cohesive laws provide more details on the strength and extensibility of the adhesive, as well as insights into the molecular mechanisms of adhesion. Moreover, cohesive laws can be directly imported into commercial finite-element software in order to model the failure of systems containing soft interfaces. The results for fibrin show that the fibrin/collagen interface is tougher than the fibrin/HAP interface which could be explained by the greater affinity of fibrin for collagen fibrils. It was also found that an increase in Ca^{2+} concentration enhances the stiffness, strength and therefore the toughness of the interface, while having no significant effect on the extensibility. However, at ~8 mM $CaCl_2$ concentration, calcium cations are detrimental to toughness and reduce the strength and extensibility of the interface. Crosslinked fibrin showed greater fracture toughness, which was attributed to greater strength and extensibility of the fibrin network and the collagen/fibrin interface due to the crosslinking. A simple failure model based on the eight-chain model was presented which could explain how the progressive failure of the bonds in the fibrin network can result in bell-shaped cohesive behavior of fibrin interfaces. The RDCB method is therefore relatively easy to implement and can yield useful information on failure mechanisms. The method can also be applied to other soft biological adhesives of importance in biological materials and structures, such as osteopontin, a biological adhesive contributing to the toughness of bone.

Acknowledgements

This work was supported by the FRSQ Network for Oral and Bone Health Research. AKD was partially supported by a McGill Engineering Doctoral Award, and MP was partially supported by the McGill Summer Undergraduate Research in Engineering program. MDM is a member of the FRSQ Groupe de Recherche Axé sur la Structure des Protéines and of the Centre for Bone and Periodontal Research. The authors wish to thank Betty Hoac for helping with the protein preparations.

Appendix A. Figures with essential colour discrimination

Certain figures in this article, particularly Figs. 1–14, are difficult to interpret in black and white. The full colour images can be found in the on-line version, at http://dx.doi.org/10.1016/j.actbio.2012.05.005.

References

[1] Smith AM, Callow JA. Biological adhesives. Berlin: Springer Verlag; 2006.
[2] Fratzl P. Nature's hierarchical materials. Prog Mater Sci 2007;52(8):1263.
[3] Fratzl P, Burgert I, Gupta HS. On the role of interface polymers for the mechanics of natural polymeric composites. Phys. Chem. Chem. Phys. 2004;6(24):5575–9.
[4] Fantner GE et al. Sacrificial bonds and hidden length dissipate energy as mineralized fibrils separate during bone fracture. Nat Mater 2005;4(8):612–6.

[5] Smith BL et al. Molecular mechanistic origin of the toughness of natural adhesives, fibres and composites. Nature 1999;399(6738):761–3.
[6] Purohit PK et al. Protein unfolding accounts for the unusual mechanical behavior of fibrin networks. Acta Biomater 2011;7(6):2374–83.
[7] Hwang DS et al. Protein- and metal-dependent interactions of a prominent protein in mussel adhesive plaques. J Biol Chem 2010;285(33):25850–8.
[8] McKee MD. Hierarchies of extracellular matrix and mineral organization in bone of the craniofacial complex and skeleton. Cells Tissues Organs 2005;181(3–4):176.
[9] Fantner GE et al. Nanoscale ion mediated networks in bone: osteopontin can repeatedly dissipate large Amounts of energy. Nano Lett 2007;7(8):2491–8.
[10] Thurner PJ et al. Osteopontin deficiency increases bone fragility but preserves bone mass. Bone 2010;46(6):1564–73.
[11] Barthelat F, Rabiei R. Toughness amplification in natural composites. J Mech Phys Solids 2011;59:829–40.
[12] Fantner GE et al. Sacrificial bonds and hidden length: unraveling molecular mesostructures in tough materials. Biophys J 2006;90(4):1411–8.
[13] Sumitomo T. In situ transmission electron microscopy observation of reversible deformation in nacre organic matrix. J Mater Res 2008;23(05):1466.
[14] Sierra DH, Eberhardt AW, Lemons JE. Failure characteristics of multiple-component fibrin-based adhesives. J Biomed Mater Res 2002;59(1):1–11.
[15] Chicot D, Démarécaux P, Lesage J. Apparent interface toughness of substrate and coating couples from indentation tests. Thin Solid Films 1996;283(1–2):151–7.
[16] Ripling EJ, Mostovoy S, Corten HT. Fracture mechanics: a tool for evaluating structural adhesives. J Adhes 1971;3(2):107–23.
[17] Zhu Y, Liechti KM, Ravi-Chandar K. Direct extraction of rate-dependent traction–separation laws for polyurea/steel interfaces. Int J Solids Struct 2009;46(1):31–51.
[18] Albala DM, Lawson JH. Recent clinical and investigational applications of fibrin sealant in selected surgical specialties. J Am Coll Surg 2006;202(4):685–97.
[19] Albala DM. Fibrin sealants in clinical practice. Cardiovasc Surg 2003;11:5–11.
[20] Ahmed T, Dare E, Hincke M. Fibrin: a versatile scaffold for tissue engineering applications. Tissue Eng B: Rev 2008;14(2):199–215.
[21] Anderson T. Fracture mechanics: fundamentals and applications. Boca Raton, FL: CRC Press; 2005.
[22] De Souza J et al. Fracture resistance curves and toughening mechanisms in polymer based dental composites. J Mech Behav Biomed Mater 2011;4:558–71.
[23] Timoshenko S. Strength of materials. New York: D. Van Nostrand; 1956.
[24] Shet C, Chandra N. Analysis of energy balance when using cohesive zone models to simulate fracture processes. J Eng Mater Tech: Trans ASME 2002;124(4):440–50.
[25] Tennent GA et al. Human plasma fibrinogen is synthesized in the liver. Blood 2007;109(5):1971–4.
[26] Scheraga HA. The thrombin–fibrinogen interaction. Biophys Chem 2004;112(2–3):117–30.
[27] Becker RC, Spencer FA. Thrombin: structure, biochemistry, measurement, and status in clinical medicine. J Thromb Thrombolysis 1998;5(3):215–29.
[28] Piechocka IK. Structural hierarchy governs fibrin gel mechanics. Biophys J 2010;98(10):2281.
[29] Fowler WE et al. Structure of the fibrin protofibril. Proc Natl Acad Sci 1981;78(8):4872–6.
[30] Weisel JW. Fibrinogen and fibrin. Adv Protein Chem 2005;70:247–99.
[31] Lorand L, Graham RM. Transglutaminases: crosslinking enzymes with pleiotropic functions. Nat Rev Mol Cell Biol 2003;4(2):140–56.
[32] Liu W et al. The mechanical properties of single fibrin fibers. J Thromb Haemost 2010;8(5):1030–6.
[33] Ryan EA et al. Structural origins of fibrin clot rheology. Biophys J 1999;77(5):2813–26.
[34] Zhu D et al. Structure and mechanical performance of a "modern" fish scale. Adv Biomater, in press.
[35] Zhu D, Vernerey F, Barthelat F. The mechanical performance of teleost fish scales. In: Proulx T, editor. Mechanics of biological systems and materials, vol. 2. New York: Springer; 2011. p. 117–23.
[36] Azzopardi PV. Roles of electrostatics and conformation in protein–crystal interactions. PLoS ONE 2010;5(2):e9330.
[37] Nakamura M. Role of blood coagulation components as intermediators of high osteoconductivity of electrically polarized hydroxyapatite. J Biomed Mater Res. B: Appl Biomater 2006;79(3):627.
[38] Zappone B et al. Effect of Ca^{2+} ions on the adhesion and mechanical properties of adsorbed layers of human osteopontin. Biophys J 2008;95(6):2939–50.
[39] Chen Y, Bal BS, Gorski JP. Calcium and collagen binding properties of osteopontin, bone sialoprotein, and bone acidic glycoprotein-75 from bone. J Biol Chem 1992;267(34):24871–8.
[40] Dang CV et al. Fibrinogen sialic acid residues are low affinity calcium-binding sites that influence fibrin assembly. J Biol Chem 1989;264(25):15104–8.
[41] Shehter-Harkavyk I, Bianco-Peled H. On the relationship between the adhesive properties and the structural features of fibrin sealants. J Adhes Sci Technol 2004;18:1415–25.
[42] Wang M-C, Pins GD, Silver FH. Preparation of fibrin glue: the effects of calcium chloride and sodium chloride. Mater Sci Eng C 1995;3(2):131–5.
[43] Collet J-P et al. The elasticity of an individual fibrin fiber in a clot. Proc Natl Acad Sci USA 2005;102(26):9133–7.
[44] James HM, Guth E. Theory of the elastic properties of rubber. J Chem Phys 1943;11(10):455–81.
[45] Arruda EM, Boyce MC. A three-dimensional constitutive model for the large stretch behavior of rubber elastic materials. J Mech Phys Solids 1993;41(2):389–412.
[46] Storm C et al. Nonlinear elasticity in biological gels. Nature 2005;435(7039):191–4.